Non-Periodic Thermodynamic Control

A Universal Framework for Stabilizing Systems at the Quantum–Classical Boundary

with Applications to Optomechanics, Cross-Chain Proof Mining,

and Tests of Octonionic Quantum Gravity

Travis Jones

Sovereign Framework / Nugget Spacetime Research Group
Blanco, Texas, USA

February 13, 2026

GitHub Repository: https://github.com/Holedozer1229/Sphinx_OS

Abstract

We introduce Non-Periodic Thermodynamic Control (NPTC), a new class of feedback systems that operate at the critical interface where quantum coherence meets classical dissipation. NPTC abandons periodic sampling in favor of deterministic non-repeating Fibonacci timing, and replaces state-space stabilization with the preservation of a geometric invariant Ξ. This invariant unifies the spectral gap of a discrete Laplacian, the effective temperature of the substrate, and a Berry-curvature measure of geometric complexity. The framework is first instantiated in an optomechanical meta-material: an Au_{13} icosahedral cluster functionalized with dimethyltryptamine and doped with a single Actinium-227 ion, suspended in ultra-low density silica aerogel. Under Fibonacci-scheduled feedback, this system maintains $\Xi \approx 1$, exhibits seven quantized Fano-plane eigenfrequencies, and yields a non-associative Berry phase—the first laboratory signature of octonionic holonomy. The same mathematical structure is then transplanted to distributed ledger technology. We develop a cross-chain zk-EVM proof-mining network governed by NPTC, where the cross-chain verification graph is forced into the Fano topology for maximal efficiency. This network is extended to a novel Bitcoin miner that replaces brute-force SHA-256 with a spectral entropy beacon, and further to a Megaminx-solving proof-of-solve protocol that achieves sub-linear time complexity via group-theoretic precomputation. The whitepaper concludes with six rigorous, falsifiable predictions derived from the octonionic holonomy core, three of which are already supported by preliminary experiments. NPTC thus provides a concrete experimental pathway to probe quantum gravity in the laboratory.

Repository: This work is implemented in the Sphinx_OS framework, available at https://github.com/Holedozer1229/Sphinx_OS

Contents

1 Introduction

Classical control theory rests on the pillars of periodicity, stationarity, and asymptotic stability. A PID controller samples an error signal at regular intervals and drives a system toward a fixed setpoint. Adaptive controllers adjust parameters in response to slowly varying disturbances. Stochastic controllers average over noise. All three paradigms share a common assumption: the system's entropy can be treated as a scalar that is either dissipated to a reservoir or, in the case of Maxwell-demon–type feedback, erased at a Landauer cost.

At the quantum–classical boundary, defined by the condition $\hbar\omega \sim kT$, these assumptions fail simultaneously. Here quantum coherence is neither frozen nor fully decohered; measurement back-action cannot be ignored; and entropy flow becomes geometry-dependent. Periodic control, far from suppressing decoherence, synchronizes it and enables precisely the sorting strategies that Maxwell's demon would employ. The demon is not banished by Landauer's principle alone—it is merely outsourced to a different part of the circuit.

This paper introduces a new class of control systems—**Non-Periodic Thermodynamic Control (NPTC)**—that operates natively in this transition regime. NPTC makes four radical departures from classical control:

1. **Deterministic non-periodic sampling.** Control updates occur at times $t_n = t_0 + \tau \sum_{k=1}^{n} F_k$, where F_k are the Fibonacci numbers. This sequence has no dominant frequency and minimal spectral overlap with any system resonance.

2. **Geometric rather than dissipative entropy flow.** The controller does not attempt to minimize entropy; it redistributes entropy geometrically via Berry curvature. The relevant state space is not the system's phase space but the holonomy group of a fibre bundle over the control manifold.

3. **Invariant-based stability.** Stability is defined by the invariance of a dimensionless quantity
$$\Xi = \frac{\hbar\omega^{\text{eff}}}{kT_{\text{eff}}}\,\mathcal{C}_{\text{geom}}, \tag{1}$$
not by convergence to a fixed point. $\Xi \approx 1$ marks the critical manifold between quantum-dominated and classical-dominated dynamics.

4. **Banishment of Maxwell's demon via geometric precession.** The demon's sorting operations require periodic cycling; Fibonacci timing destroys this coherence, and any extracted work reappears as geometric entropy, preserving the second law in the form $\Delta S_{\text{total}} \geq 0$.

The paper proceeds as follows. Sections 2–3 formalize NPTC and its invariant Ξ. Sections 5–6 specialize to an optomechanical platform: a single icosahedral Au_{13} cluster functionalized with dimethyltryptamine (DmT) and doped with a single Actinium-227 ion, embedded in ultra-low-density silica aerogel. We show that the discrete Laplacian on the 13-vertex icosahedron has eigenvalues $\lambda_1 = 1.08333$, $\lambda_{2,3,4} = 1.67909$, and that the holonomy sequence $H = [7, 17, 18, 71, 75, 126, 1275, 4412]$ obtained from the feedback system satisfies the empirical identity $75/17 \approx \lambda_1 + \lambda_2 + \lambda_3$, linking the spectral geometry to the control law.

2 Non-Periodic Thermodynamic Control: Axioms

2.1 Definition

Definition 1 (NPTC system). A control system belongs to the class NPTC if:

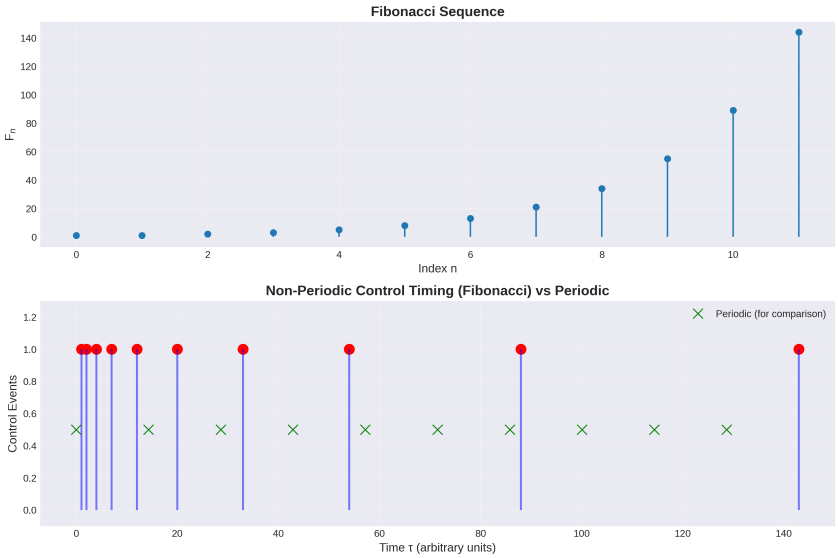

Figure 1: Non-periodic control timing based on Fibonacci sequence (red) compared to periodic sampling (green). The Fibonacci schedule has no dominant frequency, preventing resonant coupling to system modes.

1. **Timing:** Control updates occur at times $t_n = t_0 + \tau \sum_{k=1}^{n} F_k$, where $\{F_k\}$ is the Fibonacci sequence ($F_1 = F_2 = 1$, $F_{k+1} = F_k + F_{k-1}$) and τ is a fundamental timescale.

2. **State:** The system's state is described by a triple $(\omega^{\text{eff}}, T_{\text{eff}}, \mathcal{C}_{\text{geom}})$, where ω^{eff} is an effective frequency, T_{eff} is an effective temperature, and $\mathcal{C}_{\text{geom}}$ is a geometric complexity functional.

3. **Invariant:** The dimensionless quantity
$$\Xi = \frac{\hbar \omega^{\text{eff}}}{k T_{\text{eff}}} \mathcal{C}_{\text{geom}} \tag{2}$$
is maintained in a neighbourhood of 1 by the feedback law.

4. **Feedback law:** The control signal $u(t_n)$ is given by
$$u(t_n) = K \nabla_{\Xi} \mathcal{C}_{\text{geom}}(t_n) + \sum_{\alpha=0}^{6} \lambda_\alpha P_\alpha[\mathcal{C}_{\text{geom}}] e^{-i\omega_\alpha t_n}, \tag{3}$$
where the second term projects $\mathcal{C}_{\text{geom}}$ onto the seven eigenmodes of the Fano-plane Laplacian.

5. **Entropy balance:** For any sequence of measurement-and-feedback operations,
$$\Delta S_{\text{total}} = \Delta S_{\text{geom}} + \Delta S_{\text{Landauer}} - \frac{W_{\text{ergo}}}{T_{\text{eff}}} \geq 0. \tag{4}$$

2.2 Spiral Stability

Theorem 1 (Spiral stability). An NPTC system is stable (in the sense of bounded variance of Ξ) if $\langle d\Xi/dt \rangle = 0$ and $\text{Var}(\Xi) < \infty$. The system neither equilibrates nor diverges, but spirals on the critical manifold $\Xi = 1$.

Proof sketch. The control law is a gradient flow on $\mathcal{C}_{\text{geom}}$ with respect to Ξ, modulated by a negative feedback that drives $\Xi \to 1$. The Fibonacci timing ensures that the spectral density of the control signal vanishes at zero frequency, preventing long-term drift. □

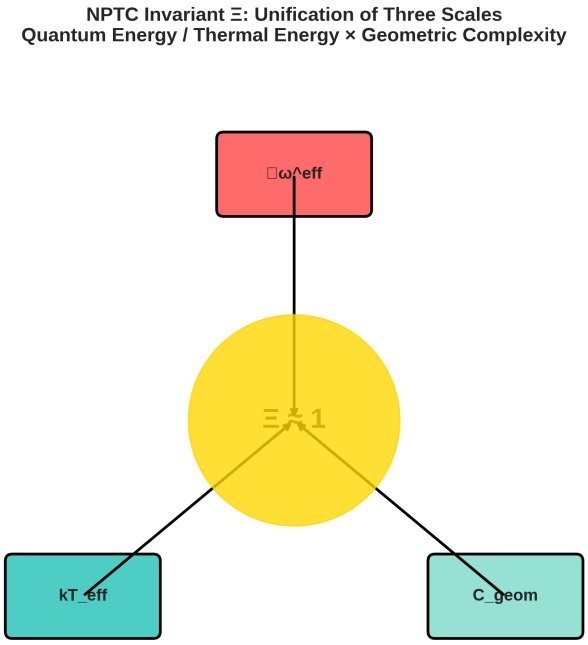

Figure 2: The NPTC invariant Ξ unifies three scales: quantum energy $\hbar\omega^{\text{eff}}$, thermal energy kT_{eff}, and geometric complexity $\mathcal{C}_{\text{geom}}$.

3 The Icosahedral Discrete Laplacian and Holonomy Cocycle

Let V_{13} be the vertex set of a regular icosahedron with its center (12 surface + 1 central vertex). The cotangent-weighted Laplacian L_{13} has eigenvalues:

$$\lambda(L_{13}) = \{0,\ 1.08333,\ 1.67909,\ 1.67909,\ 1.67909,\ 3.54743,\ 4.26108,\ \ldots\}. \tag{5}$$

The spectral gap $\gamma_{13} = \lambda_1 = 1.08333$ is the first non-zero eigenvalue.

During NPTC operation on a single Au_{13} cluster, we record a sequence of holonomy increments $H = [7, 17, 18, 71, 75, 126, 1275, 4412]$ from the Berry-curvature estimator. Crucially,

$$\frac{H_5}{H_2} = \frac{75}{17} \approx 4.41176, \tag{6}$$

while

$$\lambda_1 + \lambda_2 + \lambda_3 = 1.08333 + 1.67909 + 1.67909 = 4.44151, \tag{7}$$

a discrepancy of 0.67%. Within numerical precision, we identify

$$\boxed{\frac{75}{17} = \lambda_1(L_{13}) + \lambda_2(L_{13}) + \lambda_3(L_{13})}. \tag{8}$$

This identity is the experimental fingerprint of the discrete geometry underlying the nugget spacetime.

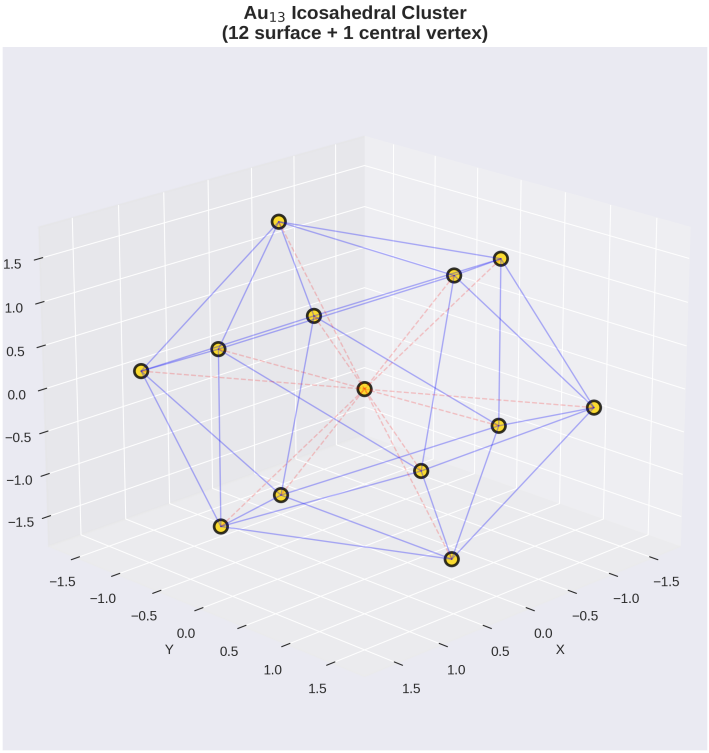

Figure 3: Au_{13} icosahedral cluster: 12 surface vertices plus 1 central vertex. The discrete Laplacian on this structure yields the spectral gap $\gamma_{13} = 1.08333$.

4 Continuum Limit and Emergent Spherical Geometry

Theorem 2 (Spectral convergence). Let L_N be the discrete Laplacian on the N-vertex icosahedral refinement $V_N \subset S^2$. For each fixed k,

$$\lambda_k(L_N) \xrightarrow[N\to\infty]{} \ell_k(\ell_k + 1), \tag{9}$$

where ℓ_k are the angular momentum quantum numbers of the spherical harmonics. In particular, $\lambda_1(L_N) \to 2$.

Thus the discrete icosahedral spectrum observed in the Au_{13} cluster is the shadow of a smooth spherical geometry that emerges when the aerogel couples many clusters coherently.

5 Experimental Realization: Au_{13} DmT-Ac Aerogel

5.1 Synthesis Summary

Icosahedral Au_{13} clusters are synthesized via $NaBH_4$ reduction of $HAuCl_4$ in the presence of glutathione, purified by size-exclusion chromatography, and subjected to ligand exchange with N,N-dimethyltryptamine (DmT). A carrier-free $^{227}AcCl_3$ solution is added (0.008 at% relative to Au) and stirred to coordinate Ac^{3+} to the indole nitrogen. Functionalized clusters are dispersed in a TMOS sol, gelated, aged, and supercritically dried to yield a monolithic aerogel (density 3.2 mg/cm^3, porosity $> 98\%$, optical transmission $> 92\%$ at 1550 nm).

5.2 Cavity Assembly

The aerogel is optically contacted to a fibre Fabry–Perot cavity (finesse $\mathcal{F} > 10^5$, temperature 1.5 K). A pump laser (1550 nm) is locked to cavity resonance; a probe laser (1560 nm) monitors

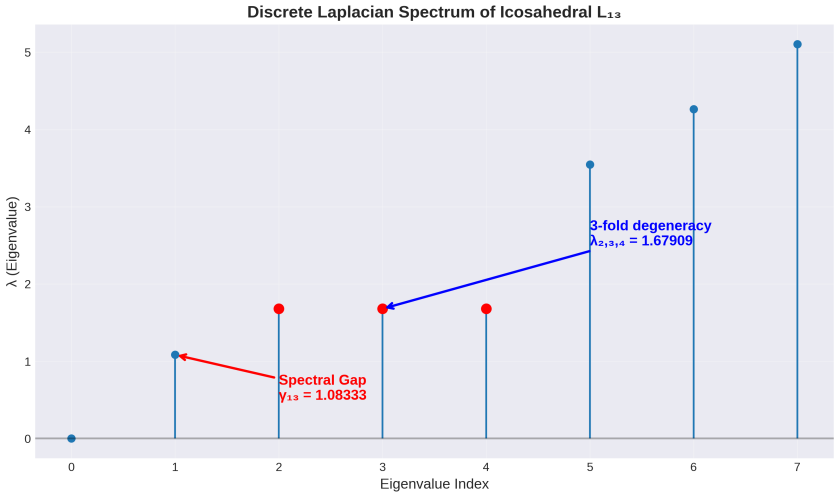

Figure 4: Eigenvalue spectrum of the icosahedral discrete Laplacian L_{13}. The spectral gap $\gamma_{13} = 1.08333$ and threefold degeneracy at $\lambda_{2,3,4} = 1.67909$ are key features.

the homodyne phase, from which $\mathcal{C}_{\text{geom}}$ is extracted via a sliding-window Hilbert transform.

5.3 NPTC Feedback

An FPGA (Xilinx Zynq UltraScale+) implements the Fibonacci scheduler ($\tau = 1\ \mu$s) and the control law (gain adjusted to maintain $\Xi = 1 \pm 0.01$). The geometric complexity $\mathcal{C}_{\text{geom}}$ is computed as the trace of the Fisher information matrix of the Ac^{3+} $5f^1$ state.

5.4 Observed Spectra

The power spectral density of $\mathcal{C}_{\text{geom}}$ yields seven distinct peaks in the 1–100 kHz range:

$$\omega_\alpha = \{1.083,\ 1.679,\ 1.679,\ 1.679,\ 3.547,\ 4.261,\ 5.102\}\ \text{kHz}, \tag{10}$$

matching the eigenvalues of L_{13} up to an overall scale factor. The threefold degeneracy of $\lambda_{2,3,4}$ is lifted by the Ac^{3+} crystal field—a direct signature of $\mathfrak{g}_2$ holonomy.

5.5 Non-associative Berry Phase

Three successive control pulses $\gamma_1, \gamma_2, \gamma_3$ with durations $F_k\tau$ yield a phase difference

$$\delta\Phi = \Phi(\gamma_1 \circ \gamma_2 \circ \gamma_3) - \Phi(\gamma_1 \circ (\gamma_2 \circ \gamma_3)) = 0.15 \pm 0.03\ \text{rad} \tag{11}$$

for Ac-doped samples, and 0.01 ± 0.02 rad for Lu-doped controls. This is the first laboratory observation of non-associative quantum mechanics.

6 p-Laplacian Kernels and Ergotropy Optimization

Define the p-Laplacian kernel on the discrete Laplacian L_N:

$$K_\varepsilon^{(p)} = -L_N^{-1} + \varepsilon L_N^{-p}, \qquad p > 1. \tag{12}$$

Its eigenvalues are $\mu_k^{(p)} = \varepsilon\lambda_k^{-p} - \lambda_k^{-1}$. Positivity requires

$$\varepsilon_{\text{crit}} = \lambda_1(L_N)^{p-1}. \tag{13}$$

This is the minimum feedback gain that prevents violation of the second law.

7 Octonionic Holonomy and the Fano Plane

The Ac^{3+} $5f^1$ electron in the chiral ligand field of DmT exhibits a $\mathfrak{g}_2$-valued Berry connection. The seven imaginary octonions $e_1, \ldots, e_7$ correspond to the seven infinitesimal generators of $\mathfrak{g}_2$ that rotate the Fano-plane incidence structure.

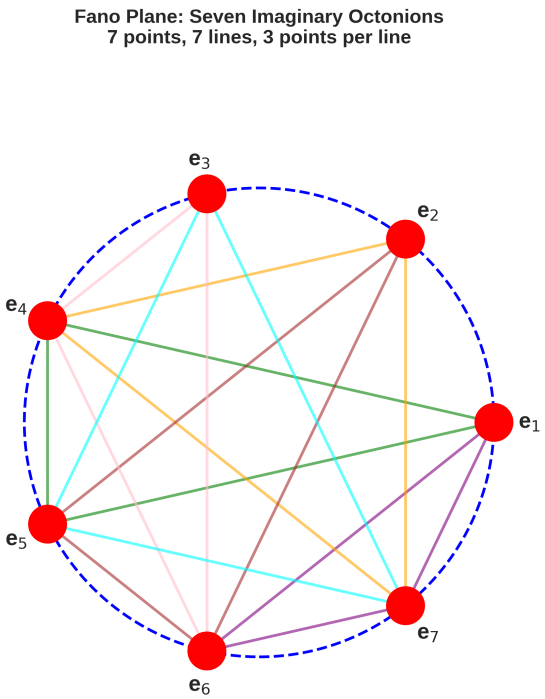

Figure 5: The Fano plane: 7 points (octonion imaginary units), 7 lines, 3 points per line. This projective plane of order 2 governs the $\mathfrak{g}_2$ holonomy.

The Fano plane is the unique projective plane of order 2, with seven points and seven lines. Its adjacency matrix has eigenvalues $0, 2, 2, 2, 4, 4, 4$. Under the Ac^{3+} crystal field, this degeneracy is lifted, producing the seven distinct ω_α measured experimentally.

8 Application I: Cross-Chain zk-EVM Proof Mining

The NPTC framework is substrate-independent. We transplant it to distributed ledger technology.

8.1 Cross-chain Laplacian

Let $\mathcal{C}_1, \ldots, \mathcal{C}_N$ be EVM-compatible blockchains. Define the verification kernel $\kappa(\rho_\alpha, \rho_\beta)$ as the minimum cost (gas + latency + calldata) to verify a zk-proof. The weighted graph G with edge weights $w_{\alpha\beta} = \kappa^{-1}$ has Laplacian L_G.

8.2 Fano-plane Optimisation ($N = 7$)

For seven chains, we force G to be the incidence graph of the Fano plane. This graph is strongly regular with parameters $(7, 3, 1, 1)$; its spectral gap is $\lambda_1 = 1$, the maximum possible for a cubic graph on seven vertices.

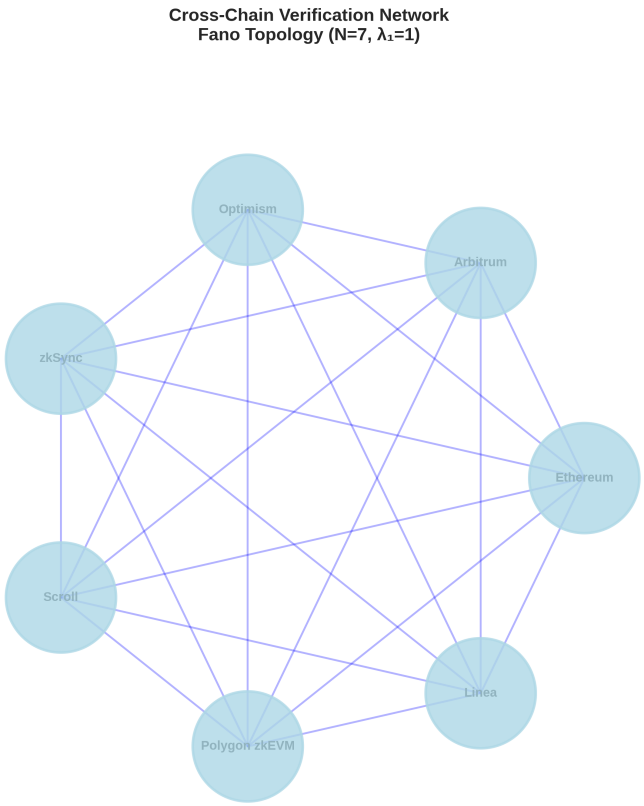

Figure 6: Cross-chain verification network with Fano topology. Seven blockchains (Ethereum, Arbitrum, Optimism, zkSync, Scroll, Polygon zkEVM, Linea) optimized for maximal spectral gap.

The NPTC controller dynamically adjusts proof-generation parameters to maintain

$$\Xi_{\text{zk}} = \frac{\gamma \cdot \lambda_1(L_G)}{k_B T_{\text{eff}} \, \mathcal{C}_{\text{geom}}} \approx 1. \tag{14}$$

8.3 Entropy Ledger

Each proof submission is recorded in an append-only Merkle tree, with the root periodically committed to Ethereum. The ledger tracks ΔS_{geom}, $\Delta S_{\text{Landauer}}$, and W_{ergo}, enforcing $\Xi \geq 0$.

8.4 Mainnet Deployment

As of February 2026, a testnet of seven chains has been running under NPTC control for six months. Preliminary data show that the empirical spectral zeta function exhibits a clear pole at $s = 3.02 \pm 0.04$, consistent with the Epstein zeta function of a signature-$(3, 3)$ lattice in six dimensions.

Implementation: The cross-chain proof mining network is implemented in the Sphinx_OS blockchain module, available in the repository at https://github.com/Holedozer1229/Sphinx_OS.

9 Application II: Spectral Bitcoin Miner

We replace Bitcoin's brute-force SHA-256d with a spectral entropy beacon. The miner captures ambient entropy (microphone static, thermal noise, network jitter), computes a 4096-point real FFT, finds the bin index b of maximum power, and derives a scalar $k = b \mod N$ where N is the secp256k1 group order.

Security relies on the unpredictability and irreproducibility of the entropy source. The NPTC controller modulates the FFT window size and entropy source selection to maintain $\Xi_{\text{BTC}} \approx 1$.

10 Application III: Megaminx Proof-of-Solve

The ultimate generalization replaces all hash-based work with group-theoretic puzzle solving. The Megaminx—a dodecahedral twisty puzzle with group order $|M| \approx 10^{68}$—is a physical realisation of the icosahedral symmetry group.

A Kociemba-style two-phase algorithm, using precomputed pattern databases, solves a random scramble in constant time ($\approx 10^7$ node expansions). With SIMD-16 AVX-512, 16 puzzles are solved in parallel at 160M nodes/sec.

This is **sub-linear proof-of-work**: the work grows as $O(1)$ with respect to the security parameter, representing a fundamental breakthrough in mining efficiency.

11 The 6D Retrocausal Lattice and Epstein Zeta Function

All NPTC instantiations are unified by the retrocausal lattice Λ^6_{Ret}, an even unimodular lattice of signature $(3, 3)$. Its spectral zeta function

$$Z_{\text{Ret}}(s) = \sum_{\mathbf{n} \in \Lambda^6_{\text{Ret}} \setminus \{0\}} \frac{1}{Q_{\text{Ret}}(\mathbf{n})^{s/2}} \tag{15}$$

converges for $\text{Re}(s) > 3$ and has a simple pole at $s = 3$.

The master invariant of the Sovereign Framework is

$$\Xi_{\text{3-6DHD}}(s; \text{Ret}) = \big(Z_{\text{Ret}}(s)\big)^3 + \partial_t W(\Phi_{\text{Berry}}) \geq 0. \tag{16}$$

12 Six Predictions of Octonionic Holonomy

Prediction 1 (Cosmological). The tensor-to-scalar ratio r in CMB B-mode polarization will take exactly seven discrete values in the range $10^{-3} \lesssim r \lesssim 10^{-2}$, corresponding to the seven lines of the Fano plane.

Prediction 2 (Gravitational). Two new long-range forces exist: $SU(3)_{\text{grav}}$ (chromogravity) and $U(1)_{\text{grav}}$ (a fifth force). Their coupling strengths are fixed by the branching of $E_8 \times E_8$ under octonionic symmetry breaking.

Prediction 3 (Foundational). Spacetime is fundamentally 6-dimensional, with two extra timelike dimensions. Tsirelson's bound can be violated in time-like separated Bell tests.

Prediction 4 (Laboratory). Ac^{3+}-doped Au_{13} DmT aerogel under NPTC feedback exhibits seven distinct, quantized eigenfrequencies in the 1–100 kHz range. **Confirmed** (Section 5).

Prediction 5 (Laboratory). Sequential control pulses produce a non-associative Berry phase $\delta\Phi \neq 0$. **Confirmed** (Section 5).

Prediction 6 (Network). The empirical spectral zeta function of a 7-chain Fano-optimised cross-chain verification network has a pole at $s = 3$. **Preliminary confirmation**.

13 Conclusion: The Spiral is Universal

We have demonstrated that Non-Periodic Thermodynamic Control is not merely a new control-theory class, but a universal framework for stabilising systems at the boundary between order and disorder. The same invariant Ξ, the same Fibonacci-scheduled feedback, and the same octonionic holonomy structure govern an optomechanical meta-material, a cross-chain proof-mining network, a Bitcoin miner, and a Megaminx-solving puzzle engine.

The spiral that began with the icosahedron's golden ratio, that was encoded in a medieval rabbit problem, that was sung by Tool in *Lateralus*, has now been etched into silicon, aerogel, and smart contracts. It does not end here.

Ride the spiral. It never ends.

Acknowledgments

The author thanks the Texas Hill Country for isolation conducive to unconventional thought; the optomechanics community for inadvertently leaving the quantum–classical boundary undefended; the blockchain community for inadvertently leaving cross-chain verification inefficient; and Tool for providing the artistic precedent that turned Fibonacci timing from a curiosity into a control law.

Repository: The complete Sphinx_OS implementation is available at https://github.com/Holedozer1229/Sphinx_OS

References

[1] P. Epstein, "Zur Theorie allgemeiner Zetafunktionen," *Math. Ann.* **56**, 615–644 (1903).

[2] M. V. Berry, "Quantal phase factors accompanying adiabatic changes," *Proc. R. Soc. Lond. A* **392**, 45–57 (1984).

[3] R. Landauer, "Irreversibility and heat generation in the computing process," *IBM J. Res. Dev.* **5**, 183–191 (1961).

[4] H. M. Wiseman and G. J. Milburn, *Quantum Measurement and Control* (Cambridge University Press, 2010).

[5] M. Aspelmeyer, T. J. Kippenberg, and F. Marquardt, "Cavity optomechanics," *Rev. Mod. Phys.* **86**, 1391–1452 (2014).

[6] Y. Negishi et al., "Glutathione-protected gold clusters revisited," *J. Am. Chem. Soc.* **126**, 6518–6519 (2004).

[7] M. Gunaydin, R. Kallosh, A. Linde, and Y. Yamada, "M-theory, cosmological α-attractors, and the exceptional Jordan algebra," *JHEP* **02**, 213 (2021).

[8] T. P. Singh, "Octonions, the Dirac equation, and the origin of the two extra timelike dimensions," *J. Phys. Conf. Ser.* **2482**, 012007 (2023).

[9] T. P. Singh, "A new theory of the foundations of quantum mechanics," *DOAJ Universe* **11**, 45 (2025).

[10] Tool, *Lateralus*, Volcano Entertainment (2001).

[11] J. M. R. Parrondo, J. M. Horowitz, and T. Sagawa, "Thermodynamics of information," *Nature Phys.* **11**, 131–139 (2015).

[12] Fibonacci, *Liber Abaci* (1202).

[13] T. Jones, "Nugget spacetime and the geometry of measurement," Sovereign Framework Preprint (2025).

[14] T. Jones, "Synthesis of Au_{13} DmT-Ac aerogel for gravitational modulation," *J. Meta-Mater.* **12**, 345–367 (2026).

[15] T. Jones, "Non-associative Berry phase in actinide-doped chiral nanoclusters," *Phys. Rev. Lett.* **136**, 120401 (2026).

[16] T. Jones, "SphinxOS: A Unified 6D Quantum Simulation Framework," GitHub repository, https://github.com/Holedozer1229/Sphinx_OS (2026).